Why does silicon have an indirect band gap?

Emily Oliphant[1], Veda Mantena,[1] Madison Brod[2], G. Jeffrey Snyder[2], Wenhao Sun[1*]
[1] Department of Materials Science, University of Michigan, Ann Arbor, Michigan 48109, United States
[2] Northwestern University, Materials Science and Engineering Evanston IL, 60208 USA

*Corresponding Author: whsun@umich.edu

Supplementary information

SI.1: Details of 1D monatomic *s* and *p* tight binding model

In this section we review the simple tight binding theory behind our model in Figure 2 of the main text. The tight binding wavefunction are the sum of *s* and *p* Bloch orbitals with their respective contribution $c_{n\alpha}^{k}$, shown in Eqn. 1, where α indicates the orbital, *n* the band, and *k* the *k*-point.

$$\Psi_n^k(r) = c_{ns}^k\,\Phi_{\mathrm{s}}(r) + c_{np}^k\,\Phi_{\mathrm{p}}(r) \tag{1.1}$$

The Hamiltonian for our system including first and second nearest neighbors is shown in Eqn. 2.

$$H = \begin{bmatrix} E_s + H_{ss}^{1NN} + H_{ss}^{2NN} & H_{sp}^{1NN} + H_{sp}^{2NN} \\ -H_{sp}^{1NN} - H_{sp}^{2NN} & E_p + H_{pp}^{1NN} + H_{pp}^{2NN} \end{bmatrix} \tag{1.2}$$

In 1D system with interatomic spacing of a, there are two 1NN at locations $+a$ and $-a$ and two 2NN at $+2a$ and $-2a$. The Brillouin zone is also limited to 1D, from Γ ($k = 0$) to *X* ($k = \frac{\pi}{a}$). Thus, the $\boldsymbol{k}\cdot\boldsymbol{R}$ term is $\pm ak$ for the 1NN and $\pm 2ak$ for the 2NN. When defining k_x from 0 at Γ to 1 at *X* the phase becomes $\pm\pi k_x$ for the 1NN and $\pm 2\pi k_x$ for the 1NN. Because each term is the sum of two opposite sign imaginary exponentials, the functional form reduces to sine for s-p bonds where the hopping parameter changes sign, and cosine for s-s and p-p bonds. The full bond runs are written below with the sign of the hopping parameter carried out to the front.

$$H_{sp}^{1NN}(k) = 2i\,\left|V_{sp}^{1NN}\right|\sin(\pi k_x)$$

$$H_{ss}^{1NN}(k) = -2|V_{ss}^{1NN}|\cos(\pi k_x)$$

$$H_{pp}^{1NN}(k) = 2\left|V_{pp}^{1NN}\right|\cos(\pi k_x)$$

$$H_{sp}^{2NN}(k) = 2i\,\left|V_{sp}^{2NN}\right|\sin(2\pi k_x)$$

$$H_{ss}^{2NN}(k) = -2|V_{ss}^{2NN}|\cos(2\pi k_x)$$

$$H_{pp}^{2NN}(k) = 2\left|V_{pp}^{2NN}\right|\cos(2\pi k_x)$$

From these, we see that H_{sp}^{1NN}, H_{ss}^{2NN}, H_{pp}^{2NN}, and H_{sp}^{2NN} bond runs all have extrema away from high symmetry points. Then the Hamiltonian is diagonalized with and without the 2NN terms. While the energy can be directly obtained in the diagonalization it can be equivalently written as the sum of the bonds as described below. The band dispersions for the 1NN and 2NN are than found as the equations below. Note that $E_n^{on+1NN}(k)$ is slightly different when the eigenvectors are calculated with the 2NN terms than without.

$$E_n^{on+1NN}(k) = c_{ns}^{k\,*}c_{ns}^{k}\left(E_s + H_{ss}^{1NN}(k)\right) + c_{np}^{k\,*}c_{np}^{k}\left(E_p + H_{pp}^{1NN}(k)\right) + c_{ns}^{k\,*}c_{np}^{k}\left(2H_{sp}^{1NN}(k)\right)$$

$$E_n^{on+1NN+2NN}(k) = E_n^{on+1NN}(k) + c_{ns}^{k\,*}c_{ns}^{k}\left(H_{ss}^{2NN}(k)\right) + c_{np}^{k\,*}c_{np}^{k}\left(H_{pp}^{2NN}(k)\right) + c_{ns}^{k\,*}c_{np}^{k}\left(2H_{sp}^{2NN}(k)\right)$$

SI.2: Comparing our 2NN model to Vogl's *sps** model

Here we compare our 1NN+2NN model, which relies crucially on the 2NN same *p* orbital bond (e.g. p_x-p_x), to the Vogl *sps** model, which also reproduces a minimum off-X for silicon. While the motivation for considering additional parameters from 1NNs is to capture the CBM off-X, the impact that the added parameter has on the rest of the band structure reveals how physical the parameter is. For physical accuracy, including an additional term into a model should qualitatively improve your fit across the entire Brillouin Zone or *k*-path. Because our model includes only 1NN and some 2NN terms from a TB interpolation of DFT band structure, it will have some quantitative error due to limiting the number of terms. While Vogl's model (which is fit only using 1NN *sps** terms) may have less quantitative error along the Γ-X line, it produces qualitatively incorrect band shapes along various *k*-paths.

To assess the physical accuracy of our model compared to *sps**, we look at changes in qualitative band shape on other *k*-paths. First examining the Γ-L line, a clear physical problem for the *sps** model, is the significant lowering of the Λ_2 band. While the DFT band structure exhibits a slight lowering close to L, the L_2 point is still significantly higher than the L_1 and L_3. But in the *sps** model, the L_2 band is lower than L_3, sitting around L_1. Because the 2NN *p-p* interaction have almost no effect on any of the bands along the Γ-L line, it can lower the X_1 point without affecting the L_2 point. Additionally, while the run of the Λ_1 band with the *sps** model is lowered near the L point, consistent with the DFT band structure, the band minimum is significantly off-L, which is not reproduced from DFT.

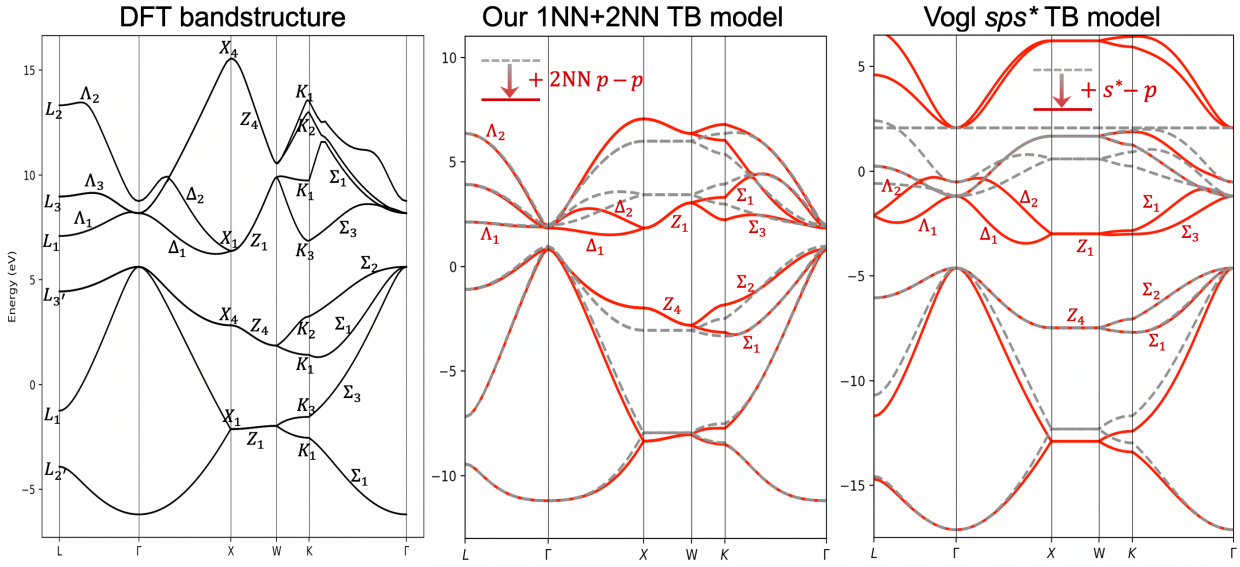

Figure SI.1: The band structures from DFT, the limited Wannier TB model, and Vogl's sps TB model are plotted. Bands and high symmetry point are labeled as needed. The TB models are plotted with (solid red) and without (dashed gray) the interaction important to the CBM near X to analyze the affect the additional term has on the band structure as a whole. Ultimately, we see the 2NN same* p-p *bond adds changes consistent with the DFT band structure, while the* s*-p *interaction creates unphysical changes.*

The other band shapes that are qualitatively changed by the *s*-p* interaction are the bottom two conduction bands along the Γ-K line, Σ_3 and Σ_1. Both of these bands with the *s*-p* interaction run down towards the K point, where the 1NN interactions mostly run up towards K (with a slight turn downwards in the Σ_1 band near K). In the DFT band structure, both bands move up from Γ to ~0.5K (Σ_3) or ~0.8K (Σ_1) than turn down sharply towards K for the remainder of the *k*-path. This matches up poorly with the *sps** model, where they run down starting at Γ (Σ_3) or ~0.3K (Σ_1) and the K_1 point is brought much lower in energy than in DFT. Including the 2NN same *p-p* interaction decreases the band energies near K while

leaving the bands largely unchanged from Γ-0.5K. While the exact shape does still not match perfectly, the decrease in the band energies only near K is seen in the DFT band structure. Thus, our 2NN same *p-p* interaction is deemed a physical correction to a 1NN model, while the extent of the *s*-p* appears unphysical.

Furthermore, there are several features in the valence bands and conduction bands of silicon which are not reproduced with a 1NN model. The 2NN same *p-p* bond address these exceptionally well, while the *s*-p* interactions have no effect. Firstly, the 1NN TB band structure is incorrectly flat along the X-W. Previously documented by Chadi and Cohen, including the 2NN same *p-p* interaction creates a dispersion along X-W which aligns well with DFT valence bands Z_1 and Z_4.[1] The added *s*-p* interaction cannot produce the dispersion from X-W, which becomes especially problematic for the conduction Z_1 band. Because the *sps** model goal is to lower the X point, it inevitably lowers the W by an equal amount. This is highly unphysical as in the DFT band structure the W_1 point is ~3 eV higher than the X_1 point. Whereas the 2NN same *p-p* orbital bond only slightly lowers the W_1 point when lowering the X_1 point. The 1NN model also poorly predicts the top two VBs along the Γ-K, Σ_1 and Σ_2, as being too close together and does not capture the low symmetry minimum off-K in the Σ_1 band. Including the 2NN same *p-p* bond fixes this, separating the K_1 and K_2 points and creating the minimum near K in the Σ_1 band, while the *s*-p* interaction has no affect.

Overall, including Vogl's *s*-p* interaction induces unphysical changes along every other high symmetry line other than Γ-X line. This reveals that within Vogl's *sps** model, the *s*-p* interaction is merely a fitting term which solely reproduces the CBM while negatively impacting the rest of the silicon band structure. On the other hand, the 2NN same *p-p* interactions leave other high symmetry lines either unchanged or makes changes consistent with the DFT band structure. Thus, the inclusion of the 2NN same *p-p* interaction and its effect on the CBM in silicon is deemed physical.

Ultimately, we believe that while physical *s** states do impact the band structure, it is in a much less significant role than suggested by Vogl, and that the essential physics of the low symmetry CBM in silicon is reproduced without relying on excited states. The impact of excited states on the conduction bands is likely well estimated as the difference between the DFT band structure and TB models reproduced using solely a sp^3 orbital basis. This is well illustrated in Figure 1a of Ref [2] by Sanchez-Portal et. al.[2]

SI.3: Obtaining the best chemistry from Maximally Localized Wannier Functions

This section outlines the essential attributes of a "good" Wannierisation such that the resulting TB model can be used for physical intuition in the third step. For additional Wannier90 formalism and code examples the reader is deferred to the Wannier90 papers and user guide.

To achieve the correct generalizable chemical intuition, the Wannierization must be done with projections of all the outer shell atomic orbitals that are included in the pseudo-potential files. For example, Si requires s and p orbitals, while atoms like Ga or Pb require s, p, and d orbitals. In the projections block of the seedname.win file this translates to having '$l = 0;\ l = 1$' for Si and '$l = 0;\ l = 1; l = 2$' for Ga or Pb. Specifying the zaxis or xaxis is not necessary with atomic orbitals and setting the radial part is not necessary with projection on the pseudo-wavefunctions, which have no radial nodes for the outer shell orbitals which are not excited states. Setting zona to set orbital size may be necessary if the default projected atomic orbitals are much smaller or larger than the PAW pseudo-orbitals. This is increasingly important for compounds with atoms of significantly different sizes but not strictly necessary for silicon.

Projecting all the outer shell orbitals will include some of the conduction bands in the Wannierisation. This often requires a detangling of the desired bands. In the case of silicon, the bottom four conduction bands are nearly separated from the higher conduction bands (no overt band crossings) but of course still hybridizes with higher bands. Because the TB parameters have nontrivial variation ($\pm 20\%$) depending on the window selection for disentangling, it is preferable to do no disentanglement for a clear comparison to Germanium later. When comparing the TB interpolations of silicon with and without the detangling procedure, we find similar TB parameters and bandstructures for distances < 8 Angstroms. Only above this does the poor localization of the Wannier orbitals without disentanglement manifest with higher TB parameters and a bandstructure with incorrect high frequency wiggles. The disentangled bandstructure uses parameters of $\mathrm{num_{wann}} = 8,\ \mathrm{num_{bands}} = 15,\ \mathrm{dis_{win_{max}}} = 21.5,\ \mathrm{dis_{froz_{max}}} = 7.6$. The paper analysis is completed using the TB model without disentanglement because it produces the same qualitative dependencies on NN as the disentangled TB model and has reasonable quantitative accuracy up to hopping parameters with a distance of < 8 Angstrom.

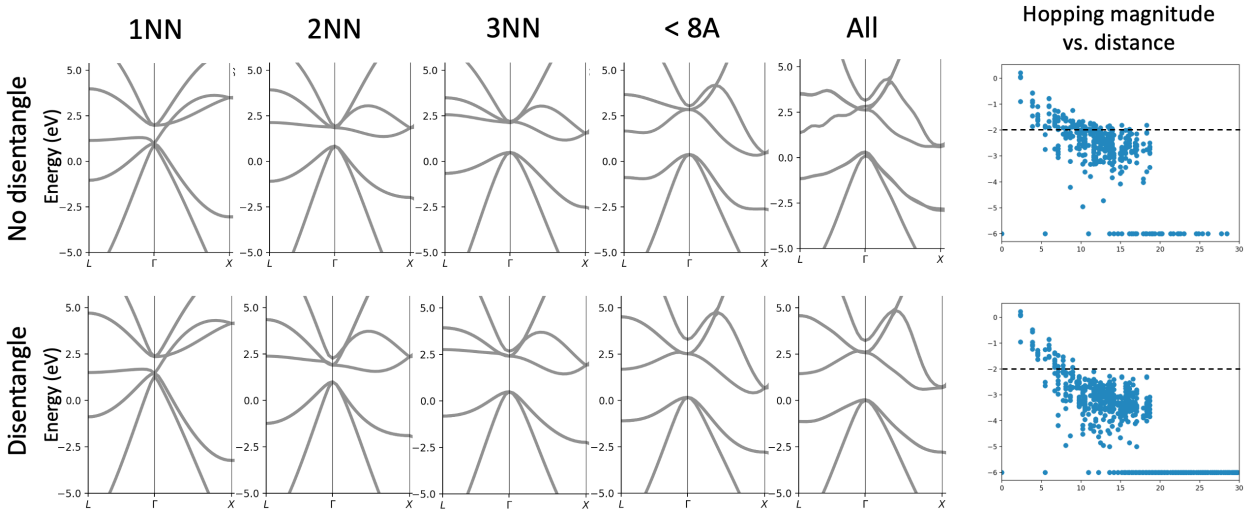

Figure SI.2: The band structures MWLF with the hopping cutoff as listed along the top for disentangling and not disentangling the bands. On the right, the log(|H|) is plotted again distance between orbitals.

Finally, check the results of the Wannierisation to determine whether it can be used to gain chemical intuition. Common metrics for a 'good' Wannierisation are that the change in spread of the Wannier

functions is <20% and that the tight binding parameters exponentially decay with distance. While these are good indicators, a change in spread of <20% is impossible with the initial projection of atomic orbitals for the Wannierisation of Si (and other covalent compounds). Atomic orbital ought to be used despite this because hybridized orbitals only work well in molecular chemistry because they are the final combination of the atomic orbitals. But in crystal, the localized orbitals combine to form a nearly infinite number of crystal orbitals across momentum space (k-space) producing a variety of hybridizations which only reduces to what human intuition might expect at limited high symmetry points. Thus, atomic orbitals must be used to clearly show the natural hybridization at any band and point in k-space. Fortunately, a precise tight binding model that maintains crystal symmetry and has near zero imaginary components can still be interpolated.

The high-quality tight binding model will be obtained when two things are true throughout the Wannierisation: the centers of the Wannier orbitals are that of the host atom in all symmetrically constrained directions, and the spread of orbitals for atoms of the same type are identical. These conditions generally need to be met immediately in the initial projection or Wannierisation tends to indirectly optimize one of the constraints at the cost of the other. For the initial projection to be good enough, I have found an odd Γ-centered *k*-point grid of the DFT calculation to be necessary. Our code requires Wannier90 output files _hr.dat, _center.xyz, and .win to generate the interactive TB band structure using a tight binding package. Then, the corresponding eigenvectors are used to determine the orbital contributions and plot the crystal wavefunctions with the e^{ikR} term using the .xsf Wannier orbital files.

Finally, our framework requires a *real*-space tight binding description of the *reciprocal*-space band structure. To apply this framework generally to materials an automated tight binding interpolation of nonorthogonal atomic orbitals from DFT needs to be realized. While MLWFs often provide a good TB interpolation, the basis set of Wannier orbitals are distorted, often significantly, from the original atomic orbitals[3,4], creating hopping parameters and coefficients which may be inconsistent with chemical intuition. On the other hand, methods that perform a TB interpolation of predefined (orthogonalized) atomic orbitals have significant errors, preventing generalization and confidence in such approaches.[5] Although the orbitals generated from MLWFs are orthogonal and vary from traditional atomic orbitals, they can still yield valuable insight when the hopping parameters produce the same sign and magnitude as from atomic orbitals.

SI.4: Visualizing chemical bonding from crystal wavefunctions of arbitrary k-points

At a low symmetry *k*-point, the long-range wavefunction in real space modulates between bonding, non-bonding, and anti-bonding. The bond-type depends on the *k*-point modulation of the atomic orbitals by the phase factor $e^{ik\cdot R_i}$. When constructing the electron density by $\psi^*\psi$, this phase factor is lost, meaning that chemical bonding (which results when atomic wavefunctions of the same phase overlap) is not a quantum mechanical observable. Hence, methods to evaluate chemical bonds using the relative energies and slopes of the charge density are necessarily indirect.

On the other hand, by constructing the supercell corresponding to a low-symmetry *k*-point, and then plotting the long-range wavefunction, we visualize chemical bonding directly. Bonding is then determined by the phase and sign of the orbitals. That is, if neighboring orbitals have orthogonal phase (e.g. real and imaginary), they do not interact and are nonbonding. Whereas when neighboring orbitals have nonorthogonal phase (e.g. real and real), they will be bonding for same-sign isosurface lobes or antibonding for opposite-sign lobes. This analysis is the same as we used for the model system in **Figure 1b**, but can now be applied to DFT calculations of materials. This brings the crystal bonding schematics used by Woodward [6], Snyder [7], and others [8–10] to a computable and generalizable scale.

This visualization is applied to Silicon in **Figure SI.3**, where the smallest supercell of the real crystal wavefunctions for three different *k*-points are plotted. Along the Δ_1 band the *s* orbital coefficient is real and positive, while the p_x orbital coefficient is imaginary and negative. To create the full wavefunction, the orbital coefficient is multiplied by the phase factor to determine the phase of the orbital on atom at center $\boldsymbol{R}$ as $c_\alpha^k\, e^{i\boldsymbol{k}\cdot\boldsymbol{R}}$ which is expanded for the Δ_1 band as $\left(\left|c_s^k\right| + i\left|c_p^k\right|\right)(\cos(\boldsymbol{k}\cdot\boldsymbol{R}) + i\sin(\boldsymbol{k}\cdot\boldsymbol{R}))$. Now, the oscillation of orbital character between *s* and p_x in the real wavefunction is seen as the *s* orbital changes as $\left|c_s^k\right|\cos(\boldsymbol{k}\cdot\boldsymbol{R})$ and the p_x orbital as $-\left|c_p^k\right|\sin(\boldsymbol{k}\cdot\boldsymbol{R})$. We plot this in the 'Total' column of **Fig 3** with vertical lines, where the color represents the *s* vs. p_x character on the atom.

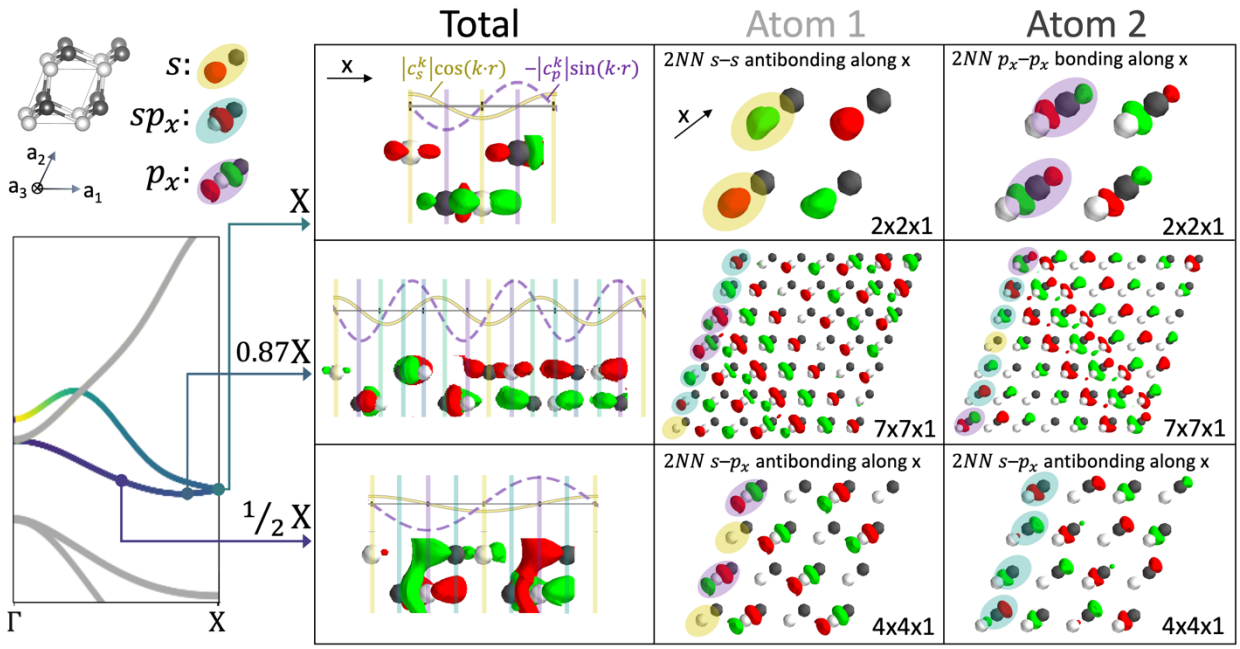

Figure SI.3: Crystal wavefunctions describe variation in 2NN bond-types along the Δ_1 band. *The orbital on an atom is colored to indicate s orbitals (yellow), sp_x hybridized orbitals (blue), and p_x orbitals (purple). Atom 1 of the two-atom basis is color white while*

Atom 2 is gray. Positive (green) and negative (red) isosurfaces of the real crystal wavefunction in their smallest repeatable supercell are plotted to inspect bond-type. The total column shows how the phase factor dictates orbital character and the other columns allow for visualizing the 2NN bond type.

To isolate the 2NN bonds, Figure 3 shows the orbitals for Atom 1 (white) and Atom 2 (gray) of the silicon primitive cell separately. The real-space oscillation in the x-direction of the conventional unit cell (corresponding to the {110} direction of the primitive cell, visualized here) reveals that only bonds with an interatomic displacement along the x-direction change bond-type along the Γ – X line. All four 1NN around an atom have the same x-translation of $|0.25a|$, while the twelve 2NNs split into eight with an x-translation of |0.5a| and four with no x-translation.

The plotted wavefunctions can be used to visually determine bond-type at specific k-points. As an example, we describe some interactions for the 2NN with an x-translation. At k = X, the alternating sign for the p_x orbitals on Atom 2 allows [red + red] or [green + green] lobes to be nearest, resulting in bonding. At k = 0.87X, the supercell size increases, each atom has a complicated mixture of orbitals, the wavelike oscillation between s and p_x orbital character is most apparent (caused by the orbital coefficients being different phases), and the p_x orbitals are bonding on average. At $k = \frac{1}{2}X$, the Atom 1 switches between s and p_x orbitals, while Atom 2 maintains sp_x orbitals. While the s orbitals on Atom 1 do not appear at this isosurface value, their sign yields antibonding. For Atom 2, the red and green sp_x lobes are always closest, also yielding antibonding. While not pictured, at k = Γ, s-s is bonding, s-p is non-bonding, and p-p is antibonding, for both 1NN and 2NN. All the s-s and s-p interactions for both 1NN and 2NN lead to a higher energy at the X point than at Γ, with the major exception of the 2NN p_x–p_x interaction—which sweeps from most antibonding at Γ to most bonding at X, resulting in a lower band energy at X.

SI.5: Derivation of final Δ_1 band dispersion

We show the full derivation and decompose of equation 6 of the main text.

The total energy of a TB wavefunction can be broken down into components from individual Bloch orbitals *i* and *j*, Eqn. 1.

$$E_n(k) = \langle \Psi_{\mathrm{nk}} | H | \Psi_{\mathrm{nk}} \rangle = \sum_{ij} {c_{ni}^k}^\dagger c_{nj}^k \, H_{ij}(k) = \sum_{ij} E_{n,ij}(k) \tag{5.1}$$

Along the Δ_1 band, there are only *s* and p_x orbitals for each atom, limiting *i* and *j* to four options. This expansion is shown by the Eqn. 2 where the superscript indicates the atom of the orbital and p_x is written as *p* for simplicity.

$$E_{\Delta_1}(k) = E_{n,s^1s^1} + E_{n,s^1p^1} + E_{n,s^1s^2} + E_{n,s^1p^2} + E_{n,p^1s^1} + E_{n,p^1p^1} + E_{n,p^1s^2} + E_{n,p^1p^2}$$
$$+E_{n,s^2s^1} + E_{n,s^2p^1} + E_{n,s^2s^2} + E_{n,s^2p^2} + E_{n,p^2s^1} + E_{n,p^2p^1} + E_{n,p^2s^2} + E_{n,p^2p^2} \tag{5.2}$$

These 16 terms are reduced considering that the coefficients for atom 1 are the same as atom 2 for the entire Δ_1 band and that atom 1 and atom 2 are the same element and thus have the same orbitals. Terms where *ji*=*ij* are also grouped together.

$$E_{\Delta_1}(k) = 2E_{n,s^1s^1} + 2E_{n,p^1p^1} + 4E_{n,s^1p^1} + 2E_{n,s^1s^2} + 4E_{n,s^1p^2} + 2E_{n,p^1p^2} \tag{3.3}$$

The 1NN interactions are between atoms 1 and 2, being the last three terms of Eqn 3, while interactions between the same atom include both the onsite (orbital energy) terms and the 2NN interactions. This equation written as onsite, 1NN, and 2NN terms is Equation 6 of the main text and Eqn. 4 below.

$$E_{\Delta_1}(k) = 2E^0_{\Delta_1,ss} + 2E^0_{\Delta_1,pp} + 2E^{1NN}_{\Delta_1,ss} + 4E^{1NN}_{\Delta_1,sp} + 2E^{1NN}_{\Delta_1,pp} + 2E^{2NN}_{\Delta_1,ss} + 4E^{2NN}_{\Delta_1,sp} + 2E^{2NN}_{\Delta_1,pp} \tag{3.4}$$

The individual terms are expanded using the bond run, where $\langle i,j \rangle$ goes over the onsite, 1NN, or 2NN bonds and $V_{ij}(\boldsymbol{R})$ is the hopping parameter.

$$E_{n,ij}(k) = {c_{ni}^k}^\dagger c_{nj}^k \, H_{ij}(k) = {c_{ni}^k}^\dagger c_{nj}^k \sum_{\boldsymbol{R}} V_{ij}(\boldsymbol{R}) e^{ik\cdot(\boldsymbol{R}+r_j-r_i)} \tag{5.5}$$

The onsite terms are most obvious, where E_s^0 is the orbital energy and $c^2 = c^\dagger c$:

$$E^0_{\Delta_1,ss} = {c^{k_x}_{\Delta_1,s}}^2 E_s^0 \tag{5.6}$$

$$E^0_{\Delta_1,pp} = {c^{k_x}_{\Delta_1,p}}^2 E_p^0 \tag{5.7}$$

1st nearest neighbors

The 1NN terms have four bonds, with $R_j - R_i$ terms of $\left[\frac{1}{4},\frac{1}{4},\frac{1}{4}\right], \left[\frac{1}{4},-\frac{1}{4},-\frac{1}{4}\right], \left[-\frac{1}{4},\frac{1}{4},-\frac{1}{4}\right], \left[-\frac{1}{4},-\frac{1}{4},\frac{1}{4}\right]$ in units of the lattice vectors $[\overrightarrow{a_1}, \overrightarrow{a_2}, \overrightarrow{a_3}]$, or denoted as $\left(\frac{1}{2},\frac{1}{2},\frac{1}{2}\right)$ in Cartesian coordinates. The Δ high symmetry line goes from [0,0,0] to [0.5,0,0.5] in units of the reciprocal lattice vectors $\left[\overrightarrow{b_1}, \overrightarrow{b_2}, \overrightarrow{b_3}\right]$ where $\overrightarrow{a_i} \cdot \overrightarrow{b_j} = 2\pi \, \delta_{ij}$. Writing $\vec{k}$ as k_x, which is 0 at Γ and 1 at *X*, we have $\sum_{1NN} V_{ij} e^{ik\cdot(\boldsymbol{R}+r_j-r_i)} = V_{ij}\left(\frac{1}{2},\frac{1}{2},\frac{1}{2}\right) e^{i\frac{k_x\pi}{2}} + V_{ij}\left(\frac{1}{2},-\frac{1}{2},-\frac{1}{2}\right) e^{-i\frac{k_x\pi}{2}} + V_{ij}\left(-\frac{1}{2},\frac{1}{2},-\frac{1}{2}\right) e^{i\frac{k_x\pi}{2}} + V_{ij}\left(-\frac{1}{2},-\frac{1}{2},\frac{1}{2}\right) e^{-i\frac{k_x\pi}{2}}$. Because *s*-*s* and *p*-*p* bonds have the same sign and magnitude for all V_{ij} while *s*-*p* has opposite sign but same magnitude we obtain Eqns 8-10 below.

$$E^{1NN}_{\Delta_1,ss} = 4{c^{k_x}_{\Delta_1,s}}^2 V_{ss}\left(\frac{1}{2}\frac{1}{2}\frac{1}{2}\right)\cos\left(\frac{k_x\pi}{2}\right) \tag{5.8}$$

$$E^{1NN}_{\Delta_1,pp} = 4{c^{k_x}_{\Delta_1,p}}^2 V_{pp}\left(\frac{1}{2}\frac{1}{2}\frac{1}{2}\right)\cos\left(\frac{k_x\pi}{2}\right) \tag{5.9}$$

$$E^{1NN}_{\Delta_1,sp} = 4{c^{k_x}_{\Delta_1,s}}^\dagger c^{k_x}_{\Delta_1,p} V_{sp}\left(\frac{1}{2}\frac{1}{2}\frac{1}{2}\right)\sin\left(\frac{k_x\pi}{2}\right) i \tag{5.10}$$

The $s - s$ ($p_x - p_x$) bond shape along the $\Gamma - \mathrm{X}$ line is a negative (positive) cosine wave with only a quarter of the cosine wavelength shown, relating to bonding (antibonding) at Γ and nonbonding at X. The $s - p_x$ bond has the shape of a quarter of a positive sine wave, with nonbonding at Γ and antibonding at X. Including the TB parameters, and the phase of the coefficients (real for s-s and p-p but imaginary for s-p), we obtain all the 1NN contributions written as Eqn. 11 below.

$$E_{\Delta_1}^{1NN}(k_x) = 2E_{\Delta_1,pp}^{1NN} + 2E_{\Delta_1,ss}^{1NN} + 4E_{\Delta_1,sp}^{1NN} \tag{5.11}$$

2nd nearest neighbors

The 2NN terms have twelve bonds, with $R_j - R_i$ terms with variations of $[\pm 1,0,0]$, $[0,\pm 1,0]$, $[0,0,\pm 1]$, $[0,\pm 1,\mp 1]$, $[\pm 1,0,\mp 1]$ and $[\pm 1,\mp 1,0]$ in lattice vectors. Of the 6 groups listed 1, 3, 4, and 6 have nonzero projections along $\Gamma \rightarrow X$ line of $\pm k_x \pi$ with bond vector denoted as (110) in Cartesian coordinates, while groups 2 and 5 have zero projection with bond vector denoted as (011) in Cartesian coordinates. Similar to the 1NN, these breakdown to cosine for s-s and p-p bonds and sine for s-p as shown in Eqns 12-14, where the extra x in the subscript denotes the TB parameters between 2NNs along the x-direction.

$$E_{\Delta_1,ss}^{2NN} = {c_{\Delta_1,s}^{k_x}}^2 [8V_{ss}(110)\cos(k_x\pi) + 4V_{ss}(011)] \tag{5.12}$$

$$E_{\Delta_1,pp}^{2NN} = {c_{\Delta_1,p}^{k_x}}^2 \left[8V_{pp}(110)\cos(k_x\pi) + 4V_{pp}(011)\right] \tag{5.13}$$

$$E_{\Delta_1,sp}^{2NN} = {c_{\Delta_1,s}^{k_x}}^{\dagger} c_{\Delta_1,p}^{k_x} \left[8V_{sp}(110)\sin(k_x\pi)\, i + 4V_{sp}(011)\right] \tag{5.14}$$

Where V_{sp}^{2NN} should be zero by symmetry. The bonding for the variable eight 2NNs should have the same shapes as their 1NN counterparts but will now cover half, rather than a quarter, of the cosine or sine wave along the $\Gamma - \mathrm{X}$ line. These are written with the TB parameters and the coefficients phase to give the contribution of 2NN, which is Eqn. 15 below. Here the $p_x - p_x$ bonds dominate with larger hopping parameters and coefficients.

$$E_{\Delta_1}^{2NN}(k_x) = 2E_{\Delta_1,pp}^{2NN} + 2E_{\Delta_1,ss}^{2NN} + 4E_{\Delta_1,sp}^{2NN} \tag{5.15}$$

SI.6: Details of computational tool

The code starts from a tight binding interpolation of DFT results, requiring basic information about the primitive cell, the number of orbitals, and the tight binding (or hopping) parameters. There will be a separate hopping parameter to represent a bond between each orbital set of *i* and *j* with all possible displaces for orbital *j* of $\mathbf{R} = \mathrm{R}_1\widehat{\boldsymbol{a_1}} + \mathrm{R}_2\widehat{\boldsymbol{a_2}} + \mathrm{R}_3\widehat{\boldsymbol{a_3}}$**.** If the interpolation is good, many of the hopping parameters will be equal or equal and opposite according to the symmetry of the orbitals and crystal. To obtain the initial band structure, the TB model is solved in the standard way using the hopping parameters to constructing k-dependent Hamiltonians which are diagonalized to obtain the energies and eigenvectors (orbital coefficients).

Then, once the user selects a point, the energy contributed by each individual bond is calculated by Eqn. 1 below, combining to Equation 1 and 3 of the main text, where the second sum is over all relevant displacements **R** between orbitals *i* and *j*, often written as $\langle i, j \rangle$.

$$E_n(k) = \sum_{ij} {c_{ni}^k}^\dagger c_{nj}^k \, H_{ij}(k) = \sum_{ij} {c_{ni}^k}^\dagger c_{nj}^k \sum_{\boldsymbol{R}} V_{ij}^{\boldsymbol{R}} \, e^{ik\cdot\boldsymbol{R}} \tag{6.1}$$

This creates an array with a flattened size of $i \cdot j \cdot \mathrm{R}_1 \cdot \mathrm{R}_2 \cdot \mathrm{R}_3$, where each element represents a single bond in the crystal and its corresponding value is the energy that bond contributes. This energy per bond array is sorted and equal magnitude elements are grouped into bonding groups, which includes all bonds that contribute the same amount of energy to that point on the band structure. For bonds to be grouped, their displacement must have the same magnitude when projected on *k*-point, $|k \cdot \mathbf{R}|$, in addition to having the same hopping parameter. One group of bonds will contribute a characteristic real shape to the total energy dispersion. For example, Eqns. 3.12 describes the energy for all 12 of the 2NN *s*-*s* bonds, where 8 are grouped into a cosine shape and 4 are grouped into a constant.

Finally, the band-dependent bond runs and bond energies can be plotted for each bond group using Equations 4 and 5 of the main text. This is written using the hopping parameters in Eqns. 2 and 3, where $\langle i, j, \mathbf{R} \rangle_b$ includes all the hopping parameters in bond group number *b*. While the phase of the coefficients $\frac{{c_{ni}^k}^\dagger c_{nj}^k}{|c_{ni}^k||c_{nj}^k|}$ changes gradually, if at all, along high symmetry lines, degenerate bands (and band crossing) cause significant jumps. Because of this, the band-dependent bond run for degenerate bands is plotted using the coefficient phase of only the clicked point, rather than changing the phase based on *k*-point.

$$H_{n,b}(k) \equiv \sum_{\langle i,j,\mathbf{R}\rangle_b} \frac{{c_{ni}^k}^\dagger c_{nj}^k}{|c_{ni}^k||c_{nj}^k|} V_{ij}^{\boldsymbol{R}} \, e^{ik\cdot\boldsymbol{R}} \tag{6.2}$$

$$E_{n,b}(k) = \left|c_{ni}^k\right|\left|c_{nj}^k\right| H_{n,b}(k) \tag{6.3}$$

Altogether, this process allows us to circumvent the long steps of calculating by hand the energies for a given band and high symmetry line as was done in SI3, which is even more challenging for less symmetric high symmetry paths.

SI.6: Tutorial of computational tool

General process

1. Open https://viz.whsunresearch.group/tb/, and click on point in bandstructure.
2. **Observe tables** with the orbital character and the most important bonds.
3. **Plot the bond run and energies** for the important bond groups by clicking on the row. This informs how a bond group effects the band dispersion along a given high symmetry line. The bond runs plotted will always be for the *n*th band based on the band index *n* that was selected in the first step.
4. **Edit hopping parameter** magnitudes to achieve a band structure with desired change.

Next, we analyze the Γ, X, and L points using our online tool. We show how to use our app to make figures similar to Figure 5(a-d) of the main text. Although, the band structures will not be exactly the same because the online app has a further NN cutoff than that plotted for our manuscript. Areas which are clicked or edited are highlighted in red, showing in the top left panel which point is clicked, in the bottom left panel which bond is selected to plot bond run and energy, and in the main panel which TB parameters are edited to generate the desired change in band structure.

Γ point

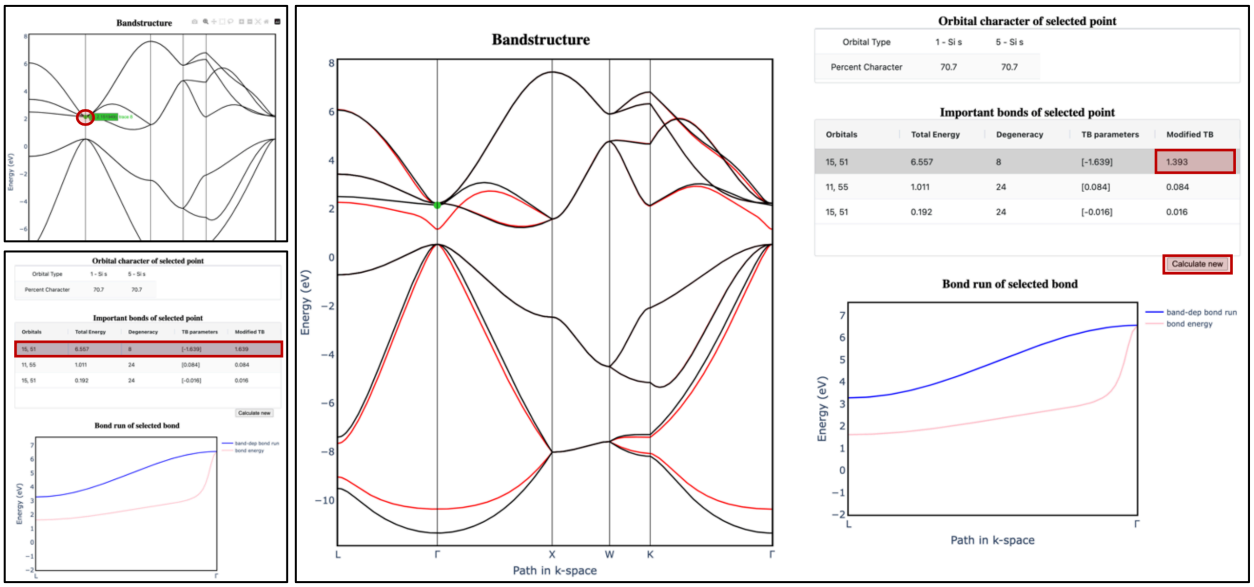

Observe tables: When the Γ point is clicked, the tables populate to reveal that the character is 50/50 Wannier orbital 1 and 5 which corresponds to the *s* orbital on atom 1 and 2. The bonds at play at this point are the 1NN, 2NN, and 3NN *s*-*s* interaction. The 1NN *s*-*s* TB parameter is –1.64 eV, in the antibonding state selected this increases the energy by 6.56 eV. The 2NN *s*-*s* TB parameter is 0.084, this is counterintuitive if the Wannier orbitals are perfect s orbitals as they should have bonding (negative) TB parameters at any distance. The positive TB parameter is reflective of the nodal behavior of Wannier orbital due to their orthogonality requirement.

Plot bond runs: In this case, the value strictly at Γ is what we are most interested in, so the bond runs play a less significant role. Particularly because the bond runs are for the highest band (rather than the lowest conduction band) along the L to Γ high symmetry line.

Edit hopping parameters: Here we want to lower the s antibonding state which was selected. We to this by reducing the TB parameter of the 1NN s-s bond by 15%. This successfully lowers *s* antibonding state while minimally effecting the energies of surrounding bands and the CBMs at the L and X points.

X point

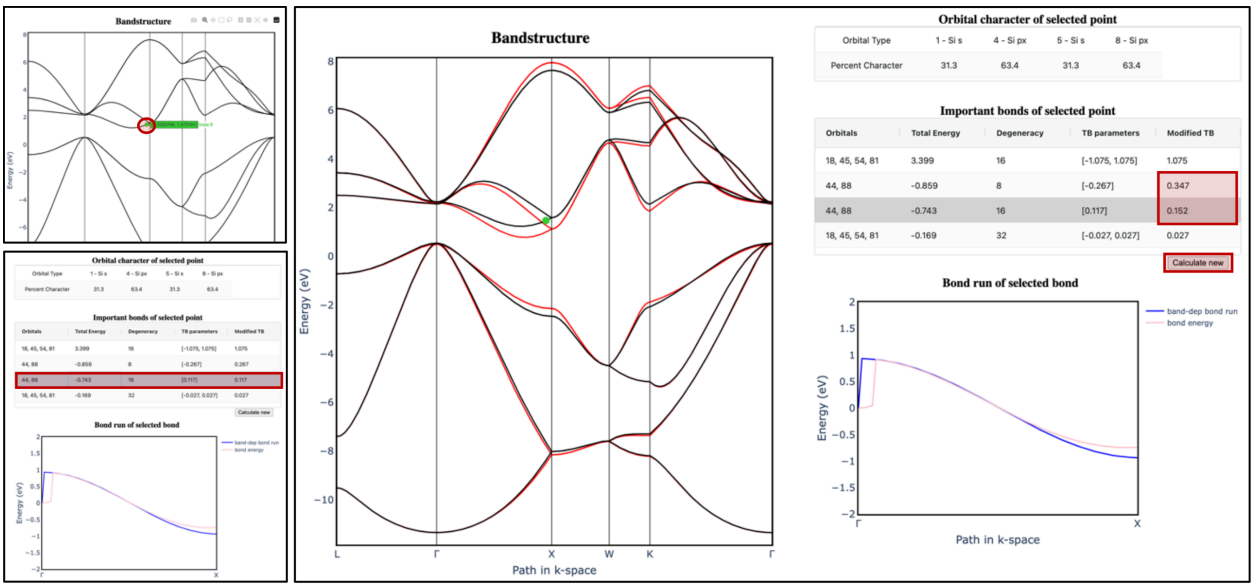

Observe tables: When near the CBM near the X point is clicked, the orbital character is shown to be *s* and p_x orbitals on atom 1 and 2 equally. The p_x orbitals have ~80% total character while the *s* orbitals have the remaining ~20%. The important bonds include (1) all the 1NN s-p bonds, (2) the 2NN *p-p* bonds without a projection on x, (3) the 2NN *p-p* bonds with a projection on *x*.

Plot bond runs: The band-dependent bond runs and bond energies will be consistent with Figure 4 and equations 7 and 8 of the main paper. With the blue lines representing the band-dependent bond runs plotted in the top of Figure 4 and the pink lines representing how the bond contributes to the total energy by scaling the bond run with the orbital character as in the middle of Figure 4.

Edit hopping parameters: With the goal of selectively lowering the X point we increase 2NN *p-p* hopping parameters by 30%. This has the desired effect because the 2NN with and without an *x* projection destructively combine at Γ, but they constructively combine near X.

L point

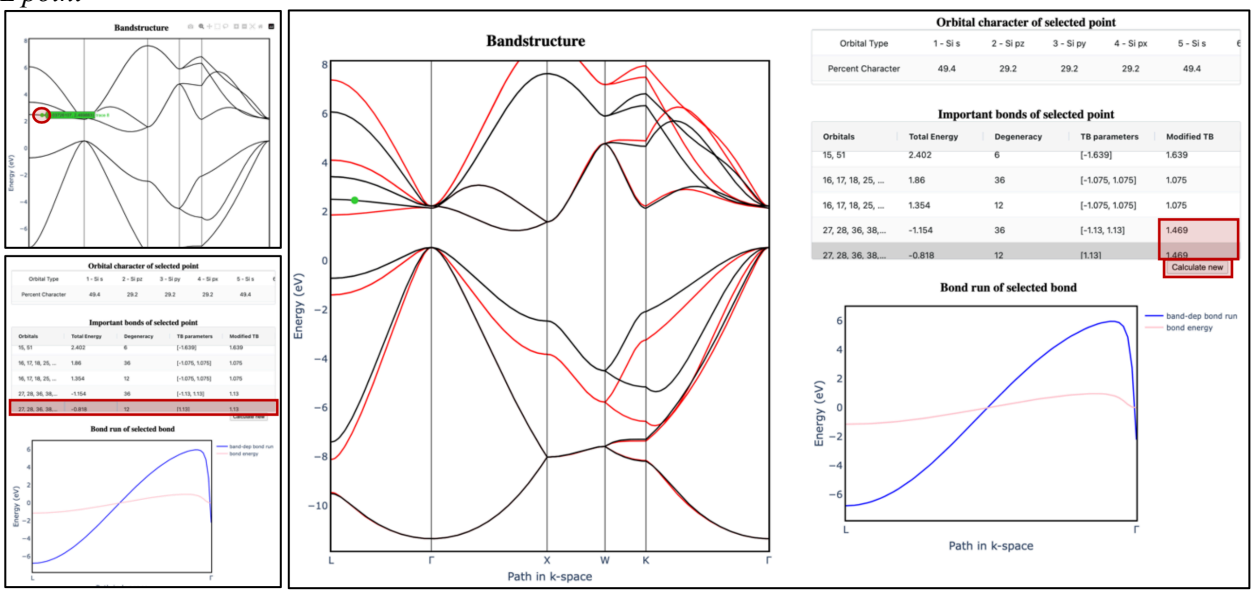

Observe tables: This band along L to Γ has character from *s, p_x, p_y*, and p_z orbitals. Atoms 1 and 2 again contribute equally and the p_x, p_y, and p_z orbitals have equal character. Much of the band is split between ~50% character *s* orbitals and ~50% character combined *p* orbitals. The diversity of orbital character increases the number of active bonds. Along the L direction, the four 1NN split into one with a nonzero projection on k-point and three with zero projection. This is distinguished in their bond run, as the bonds with zero projection are flat. The bonds contributing most to the energy at this k-point are (1) the three *s-s* bonds with zero projection (x2 for orbital variations), (2) the three *s-p* bonds (x12 for orbital variation), (3) the one *s-p* bond with a projection (x12), (4) the three *p-p* bonds (x12), (5) the one *p-p* bond with projection (x12), (6) (shown online when by scrolling) the one s-s bond with projection (x2). The extra multiplicity for the *p-p* bonds comes for the six possible combinations of different p_x-$p_{y/z}$ orbitals.

Plot bond runs: The bond runs break into ones with more # of params that are flat because the bonds have no projection along *k*-point (bonds 1, 2, and 4) and ones with less # of params which have a cosine shape (bonds 3, 5, and 6). While the first set have flat bond runs, they can have a shape in the bond energy if the orbital character changes significantly along the band. Because this band has minimal change in orbital character, the plotted bond energies remain mostly flat, except when very close to Γ.

Editing hopping parameters: With the goal of selectively lowering the L point, we target the 1NN different orbital p-p bonds by increasing them by 30%. This successfully lowers this point while have no impact on the CBM at Γ and X. This time it has no effect because there are no *p* orbitals in the antibonding *s* state at Γ and only one type of *p* orbital at the X point, restricting any different *p* orbital bonding.

SI.8: Details of Si tight binding parameters compared to Ge

The main chemical difference between silicon and germanium is the filled d shell in Ge. This introduces 10 electrons which do not fully screen the increased positive nuclear charge for the outer shell *s* and *p* orbitals. This especially impacts the *s* orbitals, which are smaller and lower in energy compared to the *p* orbitals than the *s* orbitals in silicon. This effect is often referred to as *d*-block or scandide contraction.

Because of this, we expect a rebalancing of the bond strengths to favor *p* orbitals. The *s*-*s* and possibly *s*-*p* bonds should get weaker while the *p*-*p* bonds should get stronger. Additionally, the *s* orbital energies should decrease as they are more bound. While the exact energy level cannot be compared without band alignment calculations, we can compare the energy difference between the *s* and *p* orbitals. A final note I is that the Wannier orbitals will not be exactly atomic orbitals. Because of this, the TB parameters following the developed chemical trend is obscured as the nodes near neighboring atom in the Wannier function has inconsistent effects. Still, we are able to observe the expected changes in the TB parameters. Although, this is less severe than I would anticipate for perfect atomic orbitals as the changes could be mapped onto multiple higher NN.

All of this considered, the 1NN TB parameters in eV for silicon are 1.64, 1.08, 1.13, and 0.13 for the *s*-*s*, *s*-*p*, different type *p*-*p*, and same type *p*-*p*, respectively. The *s* and *p* orbital energies are 7.12 eV apart. In germanium, the TB parameters are very similar with the largest difference occurring in the *s*-*s* hopping and *s* orbital energy difference from the *p* orbital. The parameters are 1.40, 1.03, 1.15, and 0.16 for the *s*-*s*, *s*-*p*, different type *p*-*p*, and same type *p*-*p*, respectively. The *s* and *p* orbital energies are 8.31 eV apart.

To test how these different parameters change the bandstructure, we can use our new computational tool. (Changing the orbital energy has to be done in code because it is excluded from the list of important bonds). Because we are more concerned with the accuracy of the CBM points, these bandstructures are recreated using TB parameters that are <8 Angstroms apart. Most of the change in bandstructure from silicon to germanium within the Wannierisation is caused by the *s* orbital energy that is 1.19 eV lower and the *s*-*s* bond that is 0.24 eV weaker.

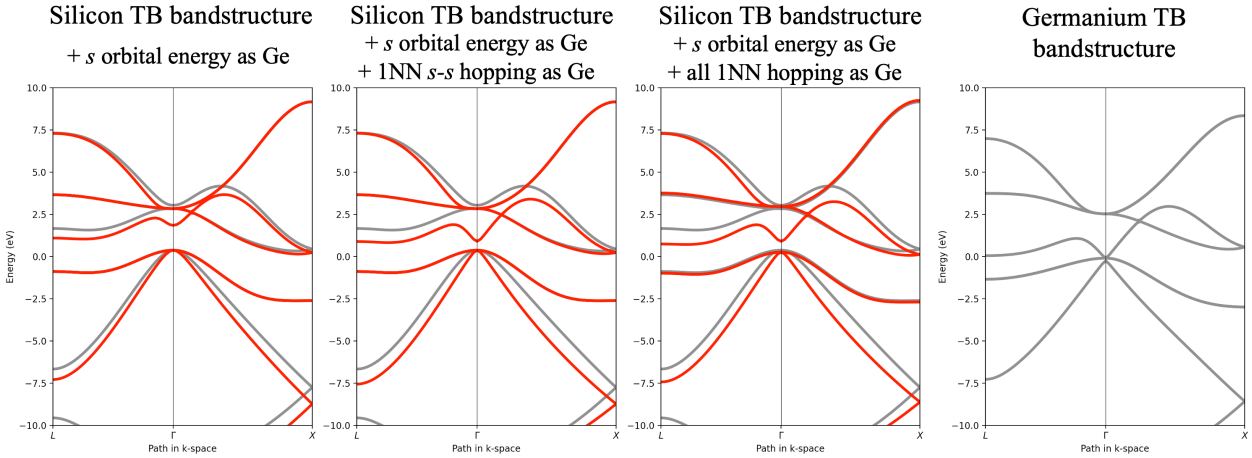

Ultimately, the Γ point is exclusively lowered by changing either the s orbital energy or s-s hopping parameters but the L and X points can be lowered through a couple chemical mechanisms, including increased *p*-*p* hopping, decreased s-p hopping, or decreased *s*-*s* hopping. While the Wannier90 results point to changes in the *s* orbital being the main cause for the onsite and 1NN terms, it is not conclusive due to the non-atomic nature of the Wannier orbitals. In other words, changes in the *p* orbitals could be mapped to the *s* orbitals as the orbitals hybridize to maintain orthogonality.

Supplementary Information References

1. Chadi, D. J. & Cohen, M. L. Tight-binding calculations of the valence bands of diamond and zincblende crystals. *Phys. Status Solidi B* **68**, 405–419 (1975).
2. Sanchez-Portal, D., Artacho, E. & Soler, J. M. Projection of plane-wave calculations into atomic orbitals. *Solid State Commun.* **95**, 685–690 (1995).
3. Marzari, N., Mostofi, A. A., Yates, J. R., Souza, I. & Vanderbilt, D. Maximally localized Wannier functions: Theory and applications. *Rev. Mod. Phys.* **84**, 1419–1475 (2012).
4. Qiao, J., Pizzi, G. & Marzari, N. Projectability disentanglement for accurate and automated electronic-structure Hamiltonians. Preprint at http://arxiv.org/abs/2303.07877 (2023).
5. Sánchez-Portal, D., Artacho, E. & Soler, J. M. Analysis of atomic orbital basis sets from the projection of plane-wave results. *J. Phys. Condens. Matter* **8**, 3859–3880 (1996).
6. Mizoguchi, H., Eng, H. W. & Woodward, P. M. Probing the Electronic Structures of Ternary Perovskite and Pyrochlore Oxides Containing Sn4+ or Sb5+. *Inorg. Chem.* **43**, 1667–1680 (2004).
7. Brod, M. K., Toriyama, M. Y. & Snyder, G. J. Orbital Chemistry That Leads to High Valley Degeneracy in PbTe. *Chem. Mater.* **32**, 9771–9779 (2020).
8. Hoffmann, R. How Chemistry and Physics Meet in the Solid State. *Angew. Chem. Int. Ed. Engl.* **26**, 846–878 (1987).
9. Zeier, W. G. *et al.* Thinking Like a Chemist: Intuition in Thermoelectric Materials. *Angew. Chem. Int. Ed.* **55**, 6826–6841 (2016).
10. Mizoguchi, H. & Woodward, P. M. Electronic Structure Studies of Main Group Oxides Possessing Edge-Sharing Octahedra: Implications for the Design of Transparent Conducting Oxides. *Chem. Mater.* **16**, 5233–5248 (2004).